www.czasopisma.pan.pl PAN POLSKA AKADEMIA NAUK www.journals.pan.pl

Arch. Metall. Mater. **68** (2023), 4, 1333-1347

DOI: https://doi.org/10.24425/amm.2023.146199

M.C. PRAVIN[1*], S. KARTHIKEYAN[2], S. SATHYABAMA[3], S. BALAJI[4]

PREPARATION AND CHARACTERIZATION OF STAINLESS STEEL-MOLYBDENUM COMPOSITE COATINGS AND ITS EVALUATION USING IMAGE PROCESSING

The objective of this paper is to develop a Non Destructive Testing (NDT) method for the detection and classification of defects in composite materials at a micro level and to devise methodologies to analyse the corrosion resistance behavior using Scanned Electron Microscope (SEM) imagery. The defects on the Stainless Steel – Molybdenum (SS-Mo) Nanocomposite coating is estimated from their Scanning Electron Micrographs by using Image Processing algorithms. For this, the SS-Mo Nano Composite coatings are fabricated using a DC magnetron sputtering process using an indigenously prepared sputtering target. Depositions are carried out on Glass substrate for the evaluation of structural, morphological, chemical composition and corrosion resistance of the coatings prepared under different conditions (deposition of SS at 300°C and RT (Room Temperature); deposition of SS + Mo at 300°C and RT). The structural and compositional analysis performed with X-ray Diffraction (XRD) and Energy-Dispersive X-ray spectroscopy (EDX) has confirmed the formation of Stainless Steel Molybdenum Composite, when the deposition is at 300°C. The SS-Mo composite deposited at 300°C is also observed to yield high corrosion resistance of the order 0.058 mm/year. A novel texture – morphology based image feature descriptor has been proposed for corrosion resistance to evaluate the composite material in a Non-destructive manner. The analysis of SEM image of the developed coatings using the proposed feature along with machine learning algorithm reveals the superior property for SS-Mo coatings deposited at 300°C which is also demonstrated by the laboratory experiments.

Keywords: SS-Mo composite; Scanning Electron Microscope; Texture analysis; Morphological analysis

1. Introduction

Rapid development of new wear and corrosion resistance materials has emerged in many applications with attractive physical and mechanical properties. One of such composites is Metal Matrix Composites (MMCs), which provides high specific modulus, strength, and Thermal stability. Hence, international attention of the researchers is towards MMCs for aerospace, automotive and other applications. Steel-based composites are a kind of metal-matrix composites, in which steel is combined with another metal that exhibits several attractive properties. Metal Matrix Composites are composed of a metallic matrix (Al, Mg, Fe, Cu etc) and dispersed ceramic (oxide, carbides) or metallic phase (Pb, Mo, W etc). MMCs are used for Space Shuttle, commercial airliners, electronic substrates, bicycles, automobiles, golf clubs and a variety of other applications.

From a material point of view, the advantages of MMCs over the polymer matrix composites lie in their retention of strength and stiffness at elevated temperature, good abrasion, wear, creep and corrosion resistance properties [1]. Corrosion is one of the unavoidable and a common vital problem in the universal industrial divisions. Due to surface instigated defects like wear, corrosion, fatigue or fracture [2], it is obvious that most of the components undergo corrosion. In order to prevent corrosion, many methods have been developed and some of the prominent methods include protective surface coatings. There are numerous techniques to implement the protective coatings, such as plasma spraying, dip coating, electroplating, spray polymer composite coatings and physical vapour deposition methods [3]. Among the aforementioned methods, the coating of polymer composites with naturally derived fibers, (such as Ananas erectifolius) [17] or synthetic fibers (such as Kevlar) [18] have attracted a great deal of attention. However for applications that require higher wear resistance and corrosion resistance, surface engineering through physical vapour deposition techniques like sputtering is highly compatible. Sputtering is a well-established surface modifying

[1] BANNARI AMMAN INSTITUTE OF TECHNOLOGY, MECHATRONICS, INDIA
[2] THIAGARAJAR COLLEGE OF ENGINEERING, MECHANICAL ENGINEERING, INDIA
[3] THIAGARAJAR COLLEGE OF ENGINEERING, ELECTRONICS AND COMMUNICATION ENGINEERING, INDIA
[4] THIAGARAJAR COLLEGE OF ENGINEERING, CHEMISTRY, INDIA

* Corresponding author: mc.pravin@gmail.com

process that deposits a variety of materials either metal or ceramic or a combination of both over various substrates [4]. Recent research emphasized that Mg metals showed a decrease of corrosion rate with immersion time, by suggesting the formation of a protective layer on their surfaces [5]. In contrast, the corrosion current density (Icorr) derived from the Tafel plots has exhibited their corrosion resistances in order of Mg > AZ91 > AZ31 [5]. Electrochemical charge transfer resistance (Rct) and double layer capacitance measured by electrochemical impedance spectroscopy (EIS) is well in accordance with the measured Icorr. EIS measurements with time and microstructural examination of the corroded and uncorroded samples are helpful in the elucidation of results measured by electrochemical polarization.

316 L stainless steel has been used in hydraulic systems due to their good corrosion resistance in a series of severely corrosive environments, such as sea water [6]. However, the micro hardness of 316 L stainless steel is ~200 HV. Low hardness usually corresponds to the low cavitation erosion and erosion-corrosion resistance and thus, 316 L stainless steel cannot meet the service requirements in liquid and slurry environments. The microstructure, chemical composition, phase constituents and micro hardness are determined by using SEM, EDS, XRD and micro hardness tester. The cavitation erosion and erosion-corrosion experiments of the coatings are investigated using an ultrasonic vibrator and a jet erosion testing measurement in 3.5 wt% NaCl solution, respectively.

An experimental approach for the study of electrochemical characteristics of the steel thin film with a thickness of 600 nm as an electrical resistance sensor material with improved sensitivity for the corrosion rate measurement has been described [7]. The thin film was deposited onto the glass by magnetron-sputtering using carbon steel targets in an Ar atmosphere. The physical properties of fabricated thin films were investigated by the X-ray diffraction (XRD) analysis, adhesion test and Auger electron spectroscopy (AES). To ensure that the thin film could replicate the corrosion behavior of bulk steel, the electrochemical polarization tests were performed. The experimental work presented here focuses on the electrochemical corrosion properties of steel thin films. Especially the effect of an Ar pressure was examined during the deposition on the corrosion behavior of these thin films. Finally, the Thin Film Electrical Resistance (TFER) sensor was fabricated and its feasibility for corrosion monitoring was investigated. In this work, the physical and corrosion properties of a sputter-deposited steel thin film as an ER sensor material were evaluated.

The role of electrochemically inactive molybdenum in alleviating the anomalous volume expansion of tin anode upon charge-discharge cycling is investigated [8]. Results of structural and compositional analyses confirmed the presence of tin and molybdenum. The elemental ratio obtained from energy-dispersive x-ray spectroscopy confirmed the feasibility of tailoring the thin-film composition by varying the ratios of metallic elements present in the sputtering target. Scanning electron micrographs of the samples revealed the occurrence of flower-like open morphology with Mo inclusion in a Sn matrix. [9,10] have investigated the microstructures of the feed stock Fe based alloy powders and the coatings by means of optical microscopy (OM), X-Ray diffraction (XRD), Thermogravimetric analysis (TGA) and Scanning Electron Microscopy (SEM). Thermally sprayed coatings are used to protect the components from different types of wear and corrosion. The current field of the application of thermal spraying includes; the oil industry to protect the component surface against a hostile environment, and automotive industry. Mostly, Fe-based metallic coating remains to form an amorphous structure showing good adhesion to the substrate.

The characterization of materials and their surface properties, such as texture and morphology, are not being considered in most of the studies. Similarly in literature, investigations of the initial stages of the corrosion reactions using advanced surface characterization techniques are scarce. [11,15] have focused to bring the importance of surface features of carbon steels, such as texture and surface energy, along with defects dislocation related to mechanical processing of carbon steels.

Most of the corrosion issues occurring in the oil and gas industries are related to pipelines and the conditions of exposure of the carbon steel that define the selection of the suitable type of carbon steel. For example, minutely added alloying elements such as Cr and Ni in carbon steels are sometimes used in the oil and gas sector. Based on the chemical composition and manufacturing procedures, different properties are gained for the steels such as texture (hot rolled texture, cold rolled texture), defects, grain sizes, dislocation densities, etc. that affect the limits of applications of the selected material.

Though there are works of literature on Metal Matrix Composites, there are depths of research on Steel Composites. Hence, Stainless steel molybdenum composites have been preferred and also this study exemplifies the importance of non-destructive techniques based on texture and morphology in analysing the corrosion rate and the results are also validated by laboratory experiments. This work focuses on establishing the role of texture in corrosion behavior of steel composites in corrosive environments, a corrosion resistance estimate directly from images with empirically derived texture features.

2. Problem formulation

In the present work, the focus is on stainless steel, molybdenum (SS-Mo) composites. Molybdenum predominantly improves the resistance towards corrosion in stainless steels as stated by [8]. Molybdenum with grades of stainless steels is usually more resistive to corrosion than molybdenum-free grades. Hence, it is used in chemical processing plants or marine applications that are more corrosive. There are several grades of stainless steels with various molybdenum contents. The suitable grade for a given application is chosen based on the corrosivity of the service atmosphere. Molybdenum, being a large atom, raises the elevated temperature strength of stainless steels through solid solution hardening. This effect is used in

heat exchangers and other elevated temperature equipment like automotive exhaust systems. This work discusses the preparation, structural characterization, Electro Chemical analysis, NDT and validation of corrosion behavior of SS-Mo composites prepared by a sputtering process which provides high corrosion resistance and increases the hardness of steel surfaces.

METHODOLOGY

Fig. 1 shows the overall methodology for the structural, compositional, morphological and corrosion analysis of Steel-Molybdenum composite.

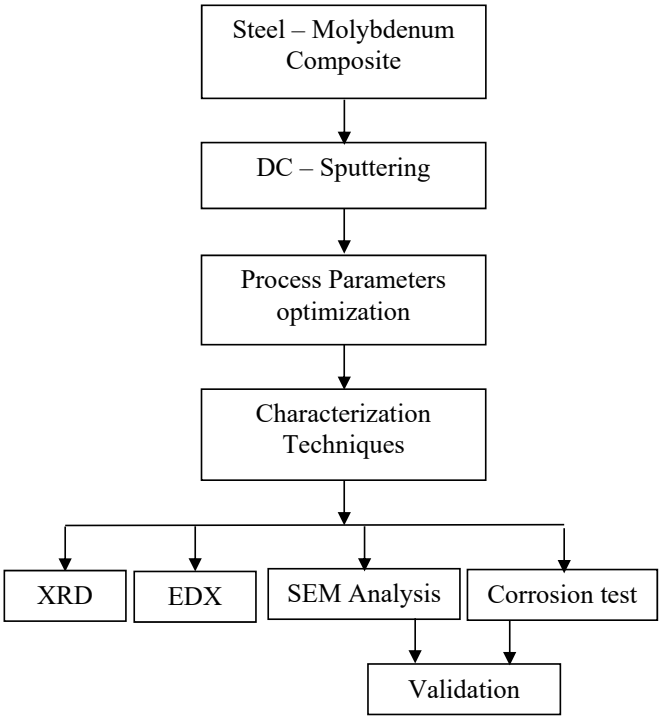

Fig. 1. Methodology for Fabrication of Thin Film Composite

Fabrication of Thin film Composites (TFC)

The thin film fabrication of Stainless steel, Molybdenum composites has been carried out using DC sputtering unit (12 inch MSPT HindHivac, India make) as shown in Fig. 2. The target for the sputtering has been indigenously designed with Stainless steel (AI304 grade) substrate (SS) and the Molybdenum embedded in the Substrate.

The composition of the stainless steel target chosen for the study has been analyzed through Energy Dispersive X ray absorption spectrometer (Bruker Make) and the results are presented in TABLE 4. As per the composition results of stainless steel, it could be observed that the SS target possess Fe (71.92%), Cr (18%) and Ni (8%) as major elements and Mn (1.31%), & C (0.77%) as minor elements. Based on the sputtering yield of Fe and Molybdenum, the sputtering target has been designed. The sputtering yields of Fe and Mo are 429 and 421 Å/minute, respectively. Since the Fe and Mo have approximately similar sputtering yields, the Fe/Mo ratio in the erosion area has been chosen as 1:1, so as to realize thin films with 1:1 Fe to Mo ratio.

TABLE 1

Composition of Stainless Steel target

Elements	Composition of stainless steel target
Iron	71.92
Chromium	18
Nickel	8
Carbon	1.31
Manganese	.77

The sputtering target has been created by tiling Mo metal sheets with an area of 9.8 cm^2, which is chopped from a 3 mm thick Mo sheet (Sigma Aldrich; Purity 99.99%) on the SS target. The depositions are carried out in Copper substrate for corrosion testing purposes and on glass substrate for structural, morphological and chemical composition characterization. Initially, the copper substrates are decreased with acetone and dipped in a NaOH solution (1 M) for 10 minutes. As the copper substrate has a natural tendency to develop surface oxides, the NaOH (sodium hydroxide) solution was used to clean the substrate Similarly, the glass substrates are pretreated with 1 N Chromic acid solution for 10 minutes and washed with double distilled water. After pre-treatment and washing, the substrates (both glass and copper) are subjected to ultra-sonication at room temperature for 30 minutes in double distilled water.

The deposition chamber, shown in Fig. 2 is emptied using a diffusion pump to a pressure level of 7×10^{-6} mbar. During thin film deposition, the chamber pressure is maintained at 0.07 mbar by purging Ar gas into the chamber at a rate of 50 sccm. The sputtering has been carried out under different conditions such as (i) deposition of SS target at room temperature (ii) deposition of SS target at 300°C, (iii) deposition of Mo embedded SS target at room temperature and (iv) deposition of Mo embedded SS target at 300°C. The stainless steel is basically an alloy of iron (Fe) and chromium (Cr). In the case of sputtering deposition, the stoichiometric composition of stainless steel varies due to the difference in sputtering yield between Fe and Cr. Hence to generate uniform nucleation on the substrate and to maintain the Fe / Cr ratio the temperature of deposition was maintained at 300°C. Moreover, from the earlier investigations of the authors, it was observed that the nucleation of molybdenum thin film also had been favoured at 300°C. Hence in this manuscript the temperature of deposition was maintained at 300°C. The other process parameters for sputtering deposition include Sputtering power, partial pressure of Argon, distance between substrate and target and they are presented in TABLE 2. The thickness of the thin film deposits is analyzed (ex-situ) using SJ 410 Mitutoyo surface profilometer. Fig. 8 shows the prepared steel molybdenum composites on copper and glass Substrate for that, the structural characterization is carried out.

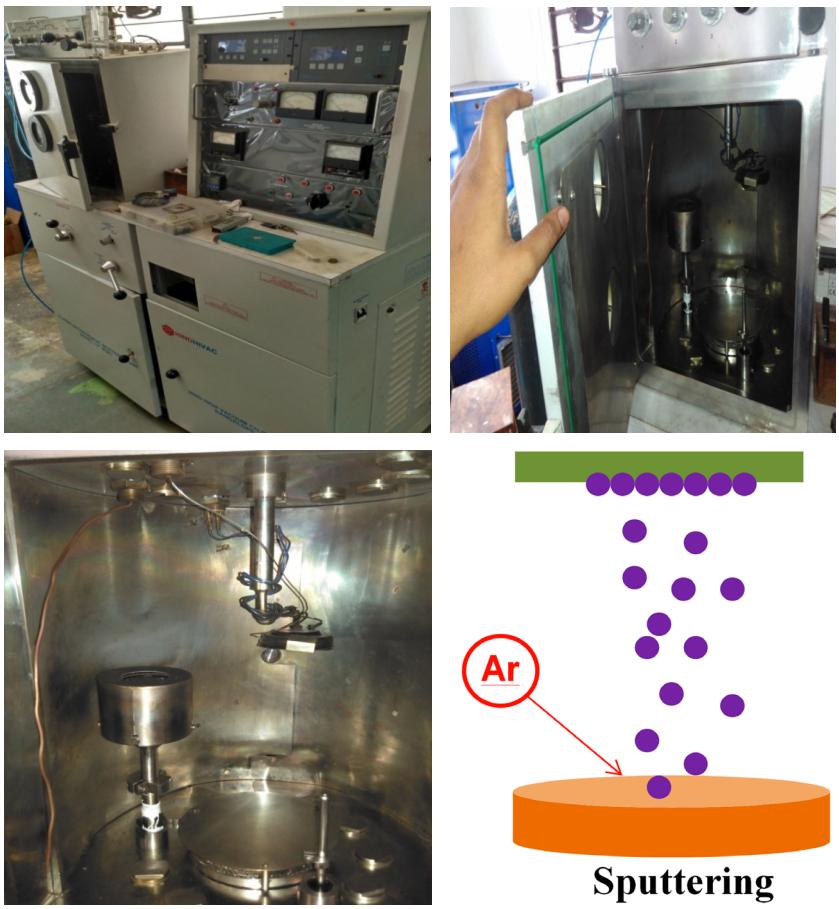

Fig. 2. DC Sputtering process

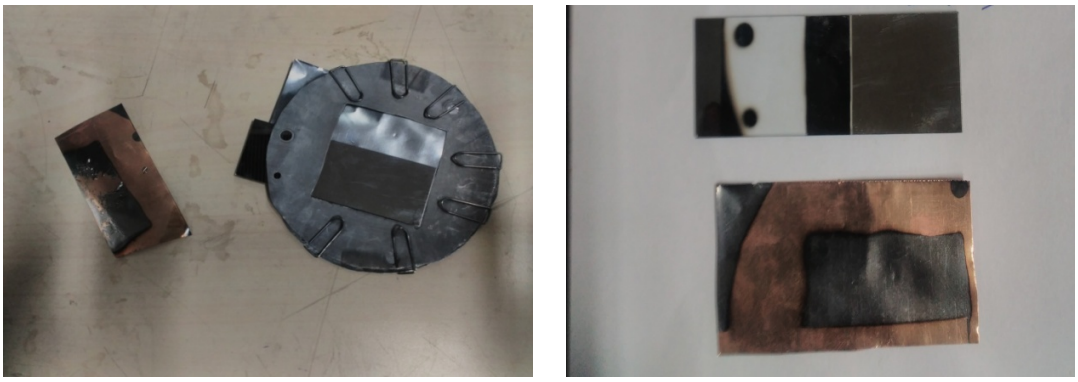

Fig. 3. Steel Molybdenum composite on Copper and Glass Substrate

TABLE 2

Process Parameters

System	Sample	
	SS Thin film	SS: Mo Thin film
Target	SS	Mo tilled SS target
Substrate	Glass and Copper substrate	Glass and Copper substrate
Supplied Power	80 W	80 W
Distance between substrate and target	4 cm	4 cm
Argon flow	50 sccm	50 sccm
Sputtering time	30 min	30 min
Deposition temperature	RT 300°C	RT 300°C
Expected composition	SS	1:1

3. Structural Characterization

The prepared thin films are subjected to structural characterization using Philips PW X ray diffractometer. The indexation of <*hkl*> peaks is carried out with reference to the ICDD database and the structural parameters like lattice parameter, lattice volume and crystallite size have been calculated using Powder X software. The lattice strain and residual stress in the thin film are also calculated using the standard formulae from the X ray diffraction pattern.

The morphological parameters of the thin films are analyzed using Tescan SBH Scanning Electron Microscope. Three representative areas are chosen in the sample scanning to understand the surface morphology. The chemical compositions of the thin films are measured using Bruker XD Energy Dispersive X ray absorption spectrometer.

IMAGE PROCESSING

SEM Image Analysis

Fig. 4 explains the step by step procedure of SEM image analysis and classifications.

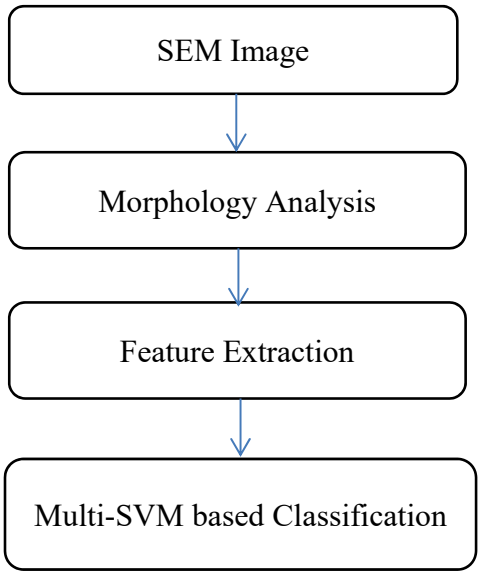

Fig. 4. Methodology for SEM analysis

SEM Image Acquisition

NDT methods that are widely used in characterizing microstructures are X-ray diffraction, Electron Microscopy (EM) including Scanning Electron Microscopy (SEM) and Transmission Electron Microscopy (TEM), and Scanning Probe Microscopy (SPM). Among these, SEM owes its popularity for the visualization of surfaces to the different types of information that it can produce, and to the fact that images and analytical information can readily be combined.

SEM analysis

The morphology and chemical composition of the fabricated specimen are investigated by Scanning Electron Microscope (SEM) which is performed on Hitachi, Japan model S-3000H instrument. The images are acquired at a resolution about 3.5 nm in size with magnifications (×1 k) having specimen size (max. 150 mm diameter) and accelerating voltage (15 KV).

4. Morphological Analysis

Morphological analysis provides information about the physical relationships of the crystalline, size, and juxtaposition of the phases present. Morphological analysis remains a predominant technique for determining the discontinuous region and the area covered by it. The specimen is said to be homogeneous only if there is less number of discontinuities, where these discontinuities occur mainly due to improper bonding, voids and pores, because of the release of a large amount of gases during the combustion process. To enhance the micro structural features, the image is pre-processed before the analysis and then, the enhanced feature is used to separate agglomerated particles or to reconstruct incomplete grain boundaries etc. Here, contrast adjustment, Thresholding and binarization are the preprocessing steps performed before morphological analysis. Then, Morphological operations like dilation and erosion have been performed with different combinations.

To determine the discontinuity, at first the Otsu thresholding is applied to the input image and it segments the image into foreground and background (Otsu 1979). Here, it has considered the grains of SS and Mo. Thresholding extracts an object from its background using a value T (threshold) for each pixel such that each pixel is classified either as an object point or a background point.

OSTU method [12] improves the image segmentation by the use of iteration approach and also minimizes intra class variance and maximizes inter class variance (Sridhar 2011). OSTU's weighted sum of variance representing intra class variance of two classes is denoted in equation (1).

$$var_w^2(T) = w_0^2(T)var_0^2(T) + w_1^2(T)var_1^2(T) \tag{1}$$

where w_0 be the probability weight of substrate and w_1 be the probability weight of coating. Threshold T separates substrate from coating by using probability weights w_0, w_1 along with their variances var_0 and var_1. $var_0(T)$ and $var_1(T)$ provide substrate and coating inter class variances.

$$\text{If} \quad var_w(T) < T \tag{2}$$

Remove unwanted regions

$$\text{If} \quad var_w(T) \geq T \tag{3}$$

Keep foreground region

Morphological operations

Morphological operations mentioned in equations 4, 5 & 6 modify the intensities of definite regions of segmented or original image. They cut off certain part of images and also expand those regions to attain a needed effect. All morphological operations use a structuring element to probe with a given input image to draw suitable conclusion [13].

$$\text{SE} = \text{strel}\,(\text{'disk'}, r, n) \tag{4}$$

Then, a disk-shaped structuring element SE is created, where r specifies the radius. n specifies the number of line structuring elements used to approximate the disk shape. Morphological operations using disk approximations run much faster, when the structuring element uses approximations.

Disk structuring element can be accomplished by performing dilation and erosion operations primarily with a 1-by-256 structuring element, and subsequently with a 256-by-1, which improves speed [13].

Dilation thickens the boundaries of an objects present in the foreground.

$$\text{dialate} = (X \oplus Y) \tag{5}$$

The dilation of set X by set Y, denoted as $X \oplus Y$, is the set union of all translations of set X by the elements of set Y.

Erosion: Shrinking the foreground

$$\text{Erode} = (X \ominus Y) \tag{6}$$

The erosion of set X by set Y, denoted as $X \ominus Y$, represents the set intersection of all negative translations of set X by the elements of set Y.

After applying the morphological operation, the resultant images taken as input image of feature extraction, tamura texture features and geometric features are extracted.

Feature Extraction and Selection

The electrochemical and corrosion behaviours of a surface are extremely complicated and they depend on various chemical, physical and mechanical factors. These factors can be directly related to the texture and geometric features of a surface and they are analyzed using SEM images. The SEM images of the samples prepared at Room Temperature (RT) and 300°C are analysed for corrosion rate in this proposed NDT method. There are various texture features developed earlier for different applications. Some of the popular texture feature extraction methods have been already discussed and studied for steel surface in the previous chapter. This work investigates texture features specifically for analysing corrosion behaviour of stainless steel composites. A corroded surface will have different surface properties including contrast, coarseness, roughness, homogeneity, compactness, porosity, convexity, solidity, energy, correlation, eccentricity etc., Among these, the feature, which contributes more for corrosion, has been selected based on experts knowledge and with an experiment. Based on this, contrast, coarseness, roughness, porosity and compactness have been selected as the most contributing features.

Coarseness (F_{crs}) relates to the distances of notable spatial variations of grey levels, that is, implicitly, to the size of the primitive elements (texels) forming the texture. Ultimately, there is an impact of grain size on corrosion. For that, the coarseness feature has been selected. If the grain size is very small, that produces fine texture which results in less corrosion and if the grain size is large, the inverse effect will be noticed.

Contrast (F_{con}) measures the way in which gray levels vary in the image and to what extent their distribution is biased to black or white. If the surface contrast is more, if there are more interruptions like pores, voids and cracks which result in poor corrosion resistance.

Roughness (F_{rgh}) feature is the simple sum of the coarseness and contrast measures. Highly bonded structures will have lower coarsness, contrast, and roughness. The corroded surface will have coarser texons and so, the roughness and contrast are high. Compactness is a characteristic quantity derived by calculating image or region's area and perimeter. It expresses the complex degree of shape. Higher the bonding, higher is the compactness. More compactness results in high corrosion resistance.

Objects with porous surfaces have empty spaces or pores that allow external matter like water, air and particles to infiltrate into the object. A porous surface may allow the moisture to enter the matter, which can result in corrosion under insulation. A coating with pores and pinhole defects creates ways for corrosive fluids or aggressive chemicals to attack the substrate material and it leads to structure failure. Stainless steels are porous and thus, they have weak corrosion resistance resulting in crevice corrosion. This corrosion resistance is increased by sealing a large portion of pores. SEM image provides micro-level structural characterization of composite material surface which can be effectively used for this corrosion behaviour analysis. TABLE 3 shows the formula for compactness and porosity.

TABLE 3

Formula for Compactness and Porosity

Features	Formula
Compactness	4π. area / perimeter^2
Porosity	Pore volume / bulk volume

Feature Weighting

Most of the conventional classification algorithms either assume all features as equally important (equal weights), or do not analyze the consistency of weights assigned to features. When the features are not consistent, assigning equal weights is not a wise task. Each sample contains some information about features importance and hence, the weights are directly derived from the sample.

The goal of feature weighting methods is to determine a relevance ranking for every feature. This goal is addressed

by introducing feature weighting function which is the ratio of the contribution of each feature to the total feature contribution [19].

$$w_i = \frac{m_i}{m_i + .. + m_n} \tag{7}$$

where m_i denotes individual feature and w_i denotes the weight of the feature.

To make a correct decision, weight has to be noted whether the feature contributes directly or inversely. For this, a weighting score has been calculated. It is defined separately for features which are directly and inversely proportional to corrosion resistance. For example, here the feature compactness is directly proportional, that is, if the compactness is more its corrosion resistance is also more. The features porosity, contrast, roughness and coarseness are inversely proportional, i.e. if porosity is more, corrosion resistance will be less. The weighting scores are defined as follows:

$$\text{Weighting Score } (WS_i) = 1 - \text{Feature} \tag{8}$$

$$\text{Weighting Score } (WS_j) = = \frac{\text{actual value} - \text{min\_value}}{\text{max\_value} - \text{min\_value}} \times 100 \tag{9}$$

WS_i – Weighting Score corresponds to Inverse relation feature,
WS_j – Weighting Score corresponds to direct relation feature.

Based on the weights and weighting scores of features, the corrosion resistance is defined as follows.

$$\begin{aligned} \text{Corrosion Resistance } (CR) = {} & w1 * WS(\text{Porosity}) + \\ & + w2 * WS(\text{Roughness}) + w3 * WS(\text{Coarsesness}) + \\ & + w4 * WS(\text{Contrast}) + w5 * WS(\text{Compactness}) \end{aligned} \tag{10}$$

where $w1$ denotes the weight of porosity, $w2$ is denoted as weight of roughness, $w3$ denotes the weight of coarseness, $w4$ specifies the weight of contrast and $w5$ specifies the weight of compactness.

The corrosion resistance behaves as an integrated feature which is given as input to SVM Classifier

Multi Class SVM Classifier

Support Vector machine (SVM) is a binary classifier which defines a hyperplane for separating two classes by maximizing the distance between the hyperplane and the binary classes. Support vectors are the samples that are close to the boundary and they are employed for defining the hyperplane. Some of the problems of pattern recognition like texture classification [14] make use of SVM. SVM Maps nonlinear input data to the linear data in high dimensional space which yields good classification. Many kernels are employed to segregate the classes and the marginal distance between these classes is maximized.

Fig. 5 shows the concept of support vector machine where X1and X2 represents the set of points related to the class. Multiclass classification is also possible either by using one-to-one or one-to many. The highest output function will be determined as the winning class. Classification is performed by considering a larger number of support vectors of the training samples. The standard form of SVM is intended for two-class problems. However, in real life situations, it is often necessary to separate more than two classes at the same time. In this section, it is explored how SVM can be extended from binary problems to multi class classification problems with k classes where $k > 2$. There are two approaches, namely the one-against-one approach and the one-against-all approach 0.1 MHz to 1 MHz Hence, there are $k(k-1)/2$ decision functions for the k-class problem. Suppose $k = 15$, 105 binary classifiers need to be trained. This suggests large training time. In the classification stage, a voting strategy is used where the testing point is designated to be in a class with the maximum number of votes. The voting approach is called the Max Wins strategy. In one-against-all approach, there will be one binary SVM for each of the class to isolate the members of one class from the other class. Here, based on the corrosion resistance, the materials are classified into 4 classes. The estimated corrosion resistance is also validated by laboratory testing.

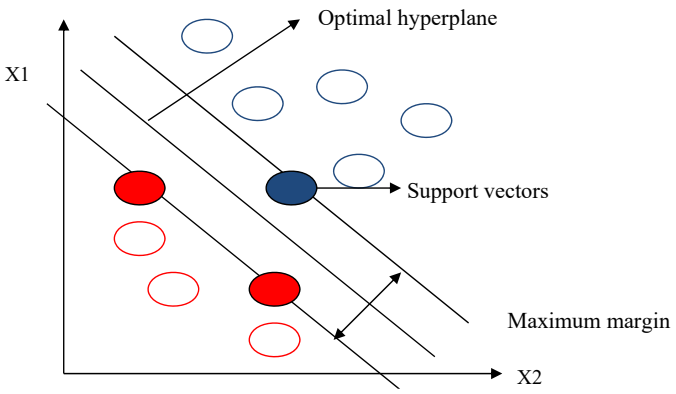

Fig. 5. Concept of Support Vector Machine

Corrosion testing

The prepared thin films have been subjected to corrosion analysis in 3.5 M NaCl solution using µAutolab III with FRA II electrochemical workstation. The Tafel polarization of the thin film samples is carried out with thin film samples as working electrodes, platinum as counter electrode and Ag/AgCl as reference electrode. The electrochemical impedance of the prepared thin films is analyzed in 3.5 M NaCl with reference to Ag/AgCl in the frequency ranging from 0.1 MHz to 1 MHz at open circuit potential. The electrochemical characterizations are performed using Autolab Frequency Response Analyser (FRA). The FRA was used to sweep the frequency from 0.1 MHz to 1 MHz. The Annual corrosion rate, electrochemical double layer capacitance and Diffusion coefficients of thin films are calculated from the Tafel polarization and Electrochemical Impedance Spectroscopy (EIS) measurements.

Fig. 6. Corrosion analysis setup

Results and Discussion

The effect of molybdenum on corrosion resistance of Fe-Mo stainless steels has been investigated. Structural and Elemental analyses have been carried out in laboratory environment for studying corrosion behavior. Non-destructive analysis of corrosion behavior has also been proposed with Scanning electron micrographs of the prepared Steel Molybdenum samples. The results are discussed in detail in the following sections.

Structural Analysis

Structural characterization is done using Philips PW X ray diffractometer. The X ray diffractograms of the thin films coated in glass substrate are presented in Fig. 7(a) to (d). From Fig. 7(a) corresponding to the thin film deposited at room temperature from SS target, it may be observed that the diffractogram possesses only one characteristic peak at 43.18 degrees barring the hump near 23 degrees. The peak near 43.18 degrees may be ascribed to Fe-C phase as per the ICDD reference 89-2005. However, other than Fe-C phase, no other element or phases have been observed. The XRD of thin film deposited at 300°C from SS target is presented in Fig. 7(b). From Fig. 7(b), similar to SS deposited at room temperature, a hump is observed near 23 degrees. However, the predominant peak is observed near 43.58 degrees and which may be ascribed to Fe-Cr-Ni-C ($FeCr_{0.29}Ni_{0.16}C_{0.06}$) phase as per ICDD reference 33-0397. Hence, it is clearly evident that the deposition of SS substrate at room temperature is devoid of Chromium and Nickel phase. From the above inference, it may also be concluded that deposition at 300°C results in composition closer to SS target.

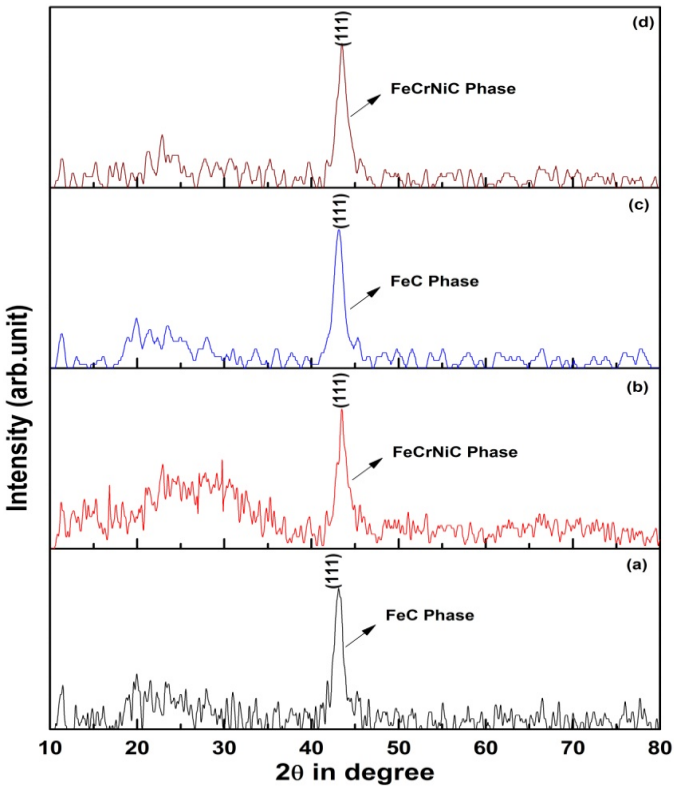

Fig. 7. (a,b,c,d) X ray Diffractometer of the thin films

In the case of deposition of Mo embedded SS target, the diffractograms of deposition at room temperature shown in Fig. 7(c & d) show the same peaks corresponding to that at 300°C observed in Fig. 7(a & b). Hence, it may be concluded that the Molybdenum remains in amorphous state between the SS layers.

The structural parameters of the deposited thin films are calculated and the results are presented in TABLE 4. From the

TABLE 4

Structural parameters

Sample	Deposition Temperature	Phase	Crystal structure	Structural Parameters		
				a	B	C
SS thin film	Room temperature	FeC	Hexagonal	4.776	4.776	4.354
SS thin film	300°C	FeCrNiC	Cubic	3.598	3.598	3.598
SS:Mo thin film	Room temperature	FeC	Hexagonal	4.776	4.776	4.354
SS:Mo thin film	300°C	FeCrNiC	Cubic	3.598	3.598	3.598
JCPDS data (File no : 892005)		FeC	Hexagonal	4.767	4.767	4.354
JCPDS data (File no 330397)		FeCrNiC	Cubic	3.591	3.591	3.591

table, it could be observed that the Fe-C phase observed in room temperature deposition possesses hexagonal structure. Due to the inclusion of Molybdenum, slight elongation in the c axis is observed. In the case of deposition at 300°C, the Fe-Cr-Ni-C phase ($FeCr_{0.29}Ni_{0.16}C_{0.06}$) with cubic crystal structure has been observed. The lattice value is identical for SS and SS-Mo composite and hence, it may be concluded that Mo exists in interstitial space between Fe-Cr-Ni-C phases.

Further to confirm the presence of Molybdenum along with SS phase, EDX analysis has been performed and the results are presented in TABLE 5. From TABLE 4, it may be observed that SS deposited at room temperature possesses Fe as a major constituent in concomitance with the target composition and it is also observed to possess Carbon up to 6.5%. However, the percentage of chromium is less compared to the SS target composition.

The SS films deposited at 300°C are observed to possess Fe and Cr as major constituents as per the target composition. However, the carbon phase could not be observed, and it may be due to the minimal percentage. The SS-Mo films deposited at room temperature have shown Fe-C phase in analogous to the results observed in the case of room temperature deposited SS films. The presence of Molybdenum could be observed in the case of SS-Mo composite thinfilm. The percentage composition of Mo is observed slightly higher than the Fe and which may be ascribed to the more preferential nucleation of Mo in the colder substrate than Fe. Though Fe and Mo have similar sputtering yields, the gas phase condensation of Mo in the colder substrate is observed to be more spontaneous than the nucleation of Fe.

The results of the chemical composition of SS-Mo composite thin film are presented in TABLE 5. It shows that the percentage composition of Fe and Mo is similar in 1:1 ratio and it is the intended work of this manuscript. Hence, it may be concluded that the sputtering deposition of Mo embedded SS target at 300°C is a facile way to develop Thin film nano composites of Fe-Cr-Ni-C and Mo phases.

Equivalent to the laboratory testing, a NDT method has been proposed for corrosion behaviour and it is verified.

Results and Discussion for SEM Image Analysis

A Non-Destructive electro chemical analysis has been investigated by S-3000H Scanning Electron Microscope by studying the texture and morphology of the SS-Mo substrate. Fig. 3.8 displays SEM micrographs of the steel – Mo composite thin films at room and elevated temperatures and in which, it can be observed that all films are Non-homogeneously distributed with grain agglomeration. The images are processed using the SEM images of samples shown in Fig. 8(a) and Fig. 8(b). The images are processed using MATLAB software. From the Figure, it can be inferred that deposition at an elevated temperature (300°C)

TABLE 5

Elemental Analysis

Sample	Substrate temperature	Composition				
		Iron	Chromium	Nickel	Manganese	Molybdenum
SS thin film	RT	72.28	17.8	7.8	2.12	0
SS thin film	300°C	72.31	17.65	7.9	2.14	0
SS:Mo thin film	RT	35.75	17.08	7.20	2.14	37.83
SS:Mo thin film	300°C	35.60	17.2	7.32	2.18	37.70

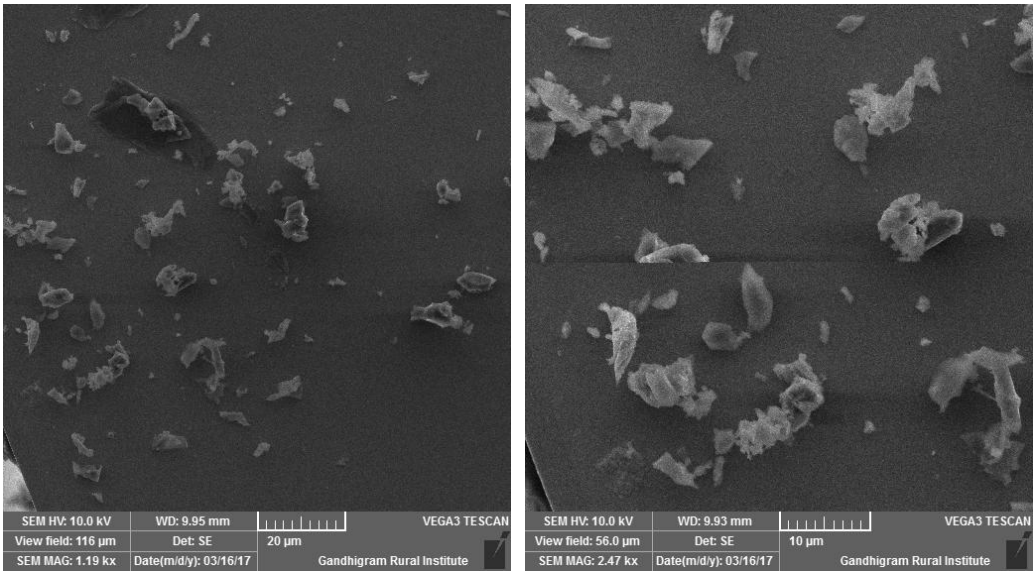

Fig. 8. (a) SEM image of SS-Mo deposited at room temperature

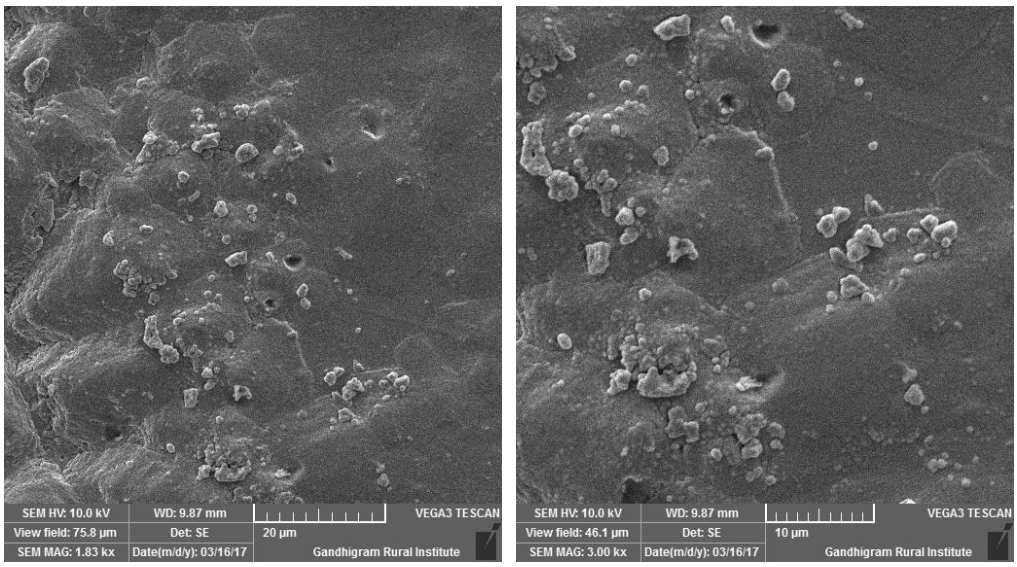

Fig. 8(b) SEM image of SS-Mo deposited at 300°C

results in less porous films compared to films deposited at room temperature.

As discussed in the previous section, after preprocessing, morphological operations, dilation erosion opening and closing have been performed with different combinations. The separated agglomerated particles with incomplete grain boundaries are reconstructed and they are shown in the Fig. 8(c).

To measure grains in a microstructure, segmentation algorithms can be designed to locate grain boundaries and label all pixels within a single continuous boundary as belonging to one grain. In this work, Morphology based segmentation has been proposed. The morphology based segmentation locates the grain boundaries and clusters all pixels within a single continuous boundary as belonging to one grain. From Fig. 8(c) it has been shown that at room temperature, the grain sizes are irregular in shpe and distributed randomly. In 300°C, the molebdynum distribution is spread over deposition of ss and the grain sizes are also of similar size which shows the compactness. From the segmented images, the texture features are extracted and they are shown in TABLE 6.

TABLE 6

Experimental results of feature extraction

		Image 1	Image 2	Image 3	Image 4	Image 5	Image 6
Contrast	**RT**	0.3663	0.5453	0.5793	0.4357	0.5299	0.8548
	300°C	0.9944	0.5639	0.8585	1.9479	1.7405	1.5214
Correlation	**RT**	0.9230	0.9442	0.9564	0.9821	0.9428	0.9483
	300°C	0.9127	0.9324	0.9363	0.8907	0.9143	0.9229
Energy	**RT**	0.8955	0.7896	0.7172	0.4948	0.8001	0.6455
	300°C	0.7477	0.8184	0.7079	0.5981	0.5514	0.5670
Homogeneity	**RT**	0.9935	0.9903	0.9897	0.9922	0.9905	0.9847
	300°C	0.9822	0.9899	0.9847	0.9652	0.9689	0.9728
Porosity	**RT**	5.2956	14.3767	20.2695	64.3659	13.3695	37.4187
	300°C	18.1339	11.1676	21.0600	36.4011	54.0257	43.1857
Solidity	**RT**	0.9318	0.8955	0.8789	0.8283	0.8931	0.8572
	300°C	0.9072	0.9198	0.9218	0.8899	0.8928	0.8945
Convexity	**RT**	0.9721	0.9398	0.9157	0.8182	0.9440	0.9140
	300°C	0.9466	0.9613	0.9605	0.9266	0.9113	0.9129
Compactness	**RT**	0.9048	0.8198	0.7797	0.5567	1.1746	0.7537
	300°C	0.9257	0.8951	0.9117	1.1280	1.0978	1.1172
Eccentricity	**RT**	0.7046	0.7187	0.6608	0.8389	0.6094	0.7715
	300°C	0.6196	0.6453	0.6531	0.6045	0.5779	0.5657
Coarseness	**RT**	0.2334	0.2205	0.2185	0.2151	0.2214	0.2184
	300°C	0.1916	0.1933	0.1914	0.1822	0.1744	0.1931
Roughness	**RT**	3.3579	2.1207	1.7865	1.0519	1.5810	0.9045
	300°C	1.0935	1.1330	0.7649	0.4145	0.3261	0.5418

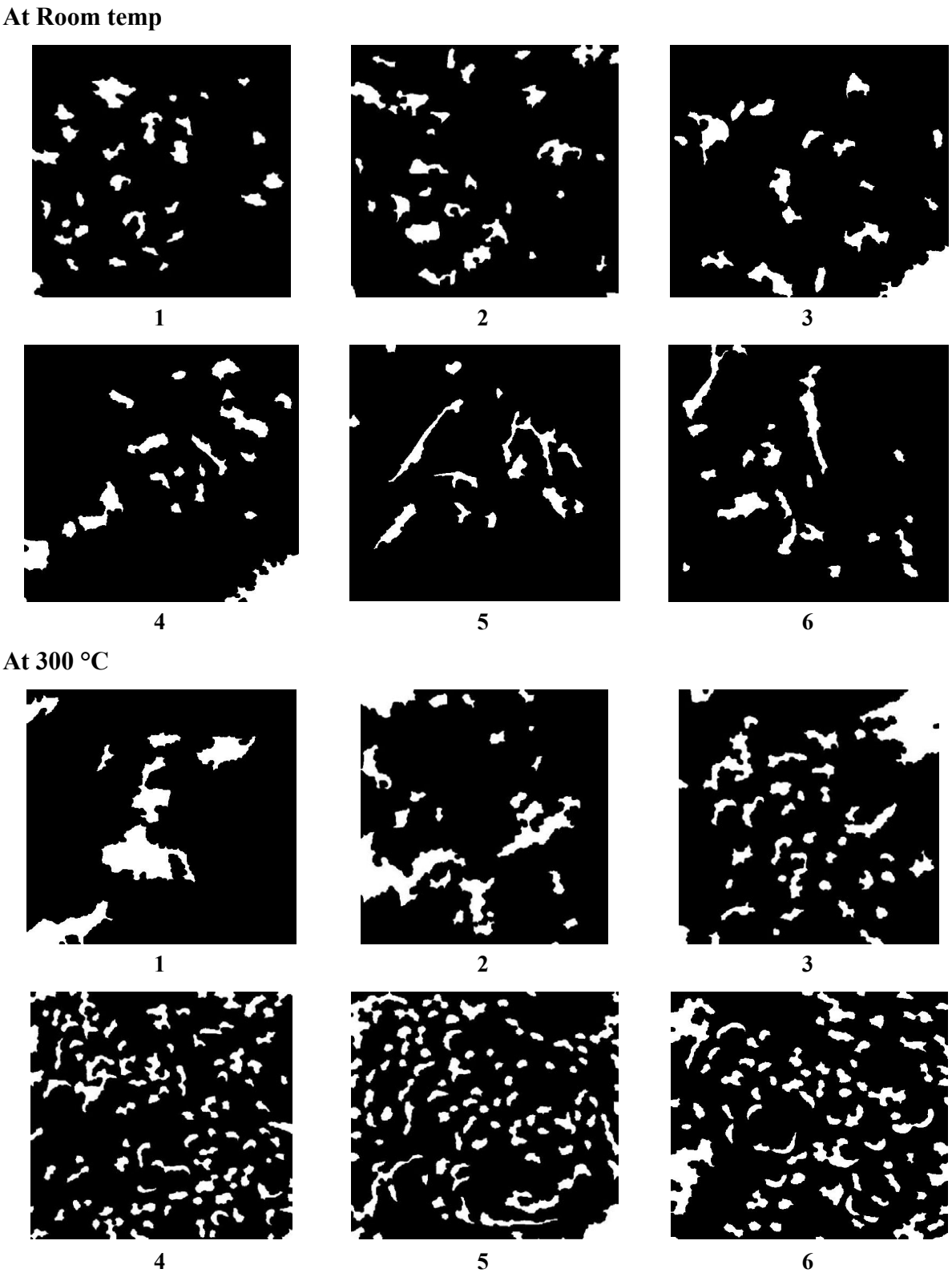

Fig. 8(c). Morphological based segmentation result

Texture based corrosion rate analysis using SEM imagery

The surface of the stainless steel greatly influences its corrosion resistance. The surface quality includes the topography of the surface, the structure and composition of the passive layer.

The effect of surface texture on the corrosion behaviour of steel solution has been investigated by texture and geometric features. TABLE 6 shows the experimental results of feature selection and the homogeneity values for image 1 at RT and at 300°C are 0.9935 and 0.9822, respectively. For image 2, the values are 0.9903 and 0.9899 f at RT and 300°C. It can be observed that

the values are highly correlated and not distinguishable between the samples of RT and 300°C. Likewise solidity, eccentricity, correlation, energy and convexity also exhibit similar values which cannot be used to make any fine decisions. But features like porosity, compactness, roughness, contrast and coarseness produce distinct values for samples taken at RT and at 300°C.

From the analysis, it is observed that the porosity of SS-Mo at Room Temperature (RT) (14.37 & 64.3659 for images 2 &4) is higher than the porosity at 300°C (11.1676 & 36.4011). It shows, if the porosity is more, the corrosion rate is also more. The compactness property at same sample at RT is .8198 & .5567 and for 300°C, it is .8951 & 1.1280, respectively. The other texture features coarseness, contrast and roughness values are high for RT than 300°C. It shows that it has less notable spatial variations than the other samples. It leads to fewer discontinuities and hence, better corrosion resistance. After feature selection, the contribution of each selected feature has been analysed for corrosion resistance with feature weighting.

Instead of giving equal importance to all the features, a feature weighting has been applied. It has been computed as the ratio of contribution of each feature to the contribution of all features. The following TABLE 1.7 shows the weights of the selected features by considering samples from SS-Mo at300°C. Almost this is same for other samples at RT also. It is noted that, the porosity plays the fore most important feature among all the bagging weights of 0.6261. Next to this, roughness, compactness and contrast contribute with less variations and coarseness contribution is small to decide the corrosion resistance. It takes the weight of 0.0204.

More weightage is given to roughness and porosity and next to this; the priorities are given to contrast, coarseness and compactness. It is also observed that the Sample without Molybdenum both at RT and 300°C, the porosity, coarseness and roughness values are high at RT than at 300°C and the compactness is more for 300°C.

Because of the relatively small number of SEM image samples, a database of Steel composites has been created as follows. It includes four categories; SS with and without Mo at RT & 300°C. An original SEM image of size 512×512 is split into non-overlapping samples of size 128X128. A set of 96 images (16×6) is formed for each category. Totally, 384 samples are formed for all the categories. The above said features are extracted for each sample. Feature weighting has been done and corrosion resistance has been calculated. It is shown in TABLE 1.8. The coarseness, contrast, roughness and porosity values are less and the compactness is more for SS-Mo at 300°C. Moreover the Temperature effect is more on corrosion resistance. The corrosion resistance capability is more for samples without Molybdenum under elevated temperature than SS with Mo at room temperature. Further, SS without Mo at room temperature exhibits poor corrosion resistance capability. It has been validated with the electrochemical analysis done at laboratory and it has been explained in further sections.

The derived CR values are given as inputs to the Multi SVM classifier which categorizes the samples based on the corrosion resistance. For the created database images, texture and geometric features are extracted. The extracted features are normalized and weighted to calculate the corrosion resistance and they serve as input to multiclass SVM (Support Vector Machine) classifier that categorizes the data as category 1,2,3 and 4 samples.

Performance Measure

To test the performance of the proposed classification of four categories of samples, the following parameters are used: Accuracy, F-score, Precision and Recall. These are calculated from confusion matrix. Precision and Recall are already explained [20].

F-Score

The F-score can be interpreted as a weighted average of the precision and recall, which can be computed by equation

$$F\text{-score} = \frac{2 * \text{precision} * \text{recall}}{\text{precision} + \text{recall}} \tag{11}$$

TABLE 7

Weights of the selected features

Features	Porosity	Roughness	Coarseness	Contrast	Compactness
Weight	0.6261	0.1313	0.0204	0.1109	0.1112

TABLE 8

Results for corrosion resistance

Features / Samples	Coarse ness	Contrast	Rough ness	Porosity	Compactness	Corrosion Resistance (CR)	Entire Image Corrosion Resistance
SS + MO 300	**0.1860**	**0.4005**	**0.5865**	**1.0526**	**1.3578**	**38.0540**	**202.81**
SS 300	0.1904	0.5076	0.6980	2.2683	1.4036	27.2494	170.71
SS + MO RT	0.2137	1.0242	1.2379	5.2560	1.3166	12.0622	172.81
SS RT	0.2222	4.9154	5.1376	6.1768	0.8319	0.6298	108.37

Accuracy

Accuracy gives the measure of overall correctness of the proposed work, and it is calculated as the sum of correct classification divided by the total number of classifications.

$$\text{Accuracy} = \frac{t_p + t_n}{t_p + t_n + f_p + f_n} \tag{12}$$

For some selected 15 textures, the proposed classification method yields a classification accuracy of 75% with a reasonable precision, recall and F-score values which are shown in TABLE 9.

TABLE 9

Performance Measure

	Precision	Recall	F-score	Accuracy
Steel Composite	42.5866	50	42.6511	75

From the proposed SEM analysis methods, it has been observed that Molybdenum increases corrosion resistance at high-temperature. Eventually, these surface modifications can influence electrochemical behaviour and, therefore corrosion susceptibility as demonstrated by the corrosion rate experiments with molybdenum at elevated temperature. This method has been validated with the laboratory electrochemical analysis which is explained in below Tafel Polarization Studies.

Tafel Polarization Studies

The results of Tafel polarization studies are presented in Fig. 9. The parameters derived from the Tafel polarization are presented in TABLE 10. From the graph, it may be observed that the samples deposited at room temperature and 300°C exhibit difference in corrosion potential (E_{Corr}). The Ecorr is observed shifting to higher potential for the thin films deposited at high temperature. This observed deviation in the corrosion potential may be corroborated to the more inert nature of the thin films. Hence, it may be concluded that the deposition of SS and SS-Mo composite films at high temperature results in better corrosion proof coatings. The corrosion rates calculated for the SS films deposited at room temperature and 300°C are 0.13 mm/year and 0.102 mm/year, respectively. Similarly, the corrosion resistances of SS-Mo thin films coated at room temperature and 300°C are 0.11 mm/year and 0.058 mm/year, respectively. Hence, the corrosion resistance of the films can be arranged in the following order. SS-Mo films deposited @ 300°C >> SS films deposited @ 300°C > SS-Mo films deposited @ RT > SS films deposited @ RT.

TABLE 10

Results for Corrosion rate

Sample	Condition	Corr Rate (mm/Year)
Sample 1	SS @ RT	0.102
Sample 2	SS @ 300°C	0.13
Sample 3	Mo and SS @ RT	0.11
Sample 4	Mo and SS @ 300°C	0.058

The mechanism behind the corrosion resistance improvement in the case of SS-Mo thin film composite is analyzed using electrochemical impedance spectroscopy and the results are presented in the form of Nyquist plot in Fig. 9. The mechanism of corrosion in SS thin film is observed to undergo two stage processes where subsequent oxidation Fe, Cr and Ni occur sequentially. Since the process occurs in two stages, the corrosion resistance will naturally be higher than Fe. The Nyquist plot of all the samples possesses two semi circles, one at higher frequency and other at lower frequency. The low frequency semi circle could be attributed to the oxidation of Cr and Ni phases in the SS and the higher frequency semi circle corresponds to Fe oxidation.

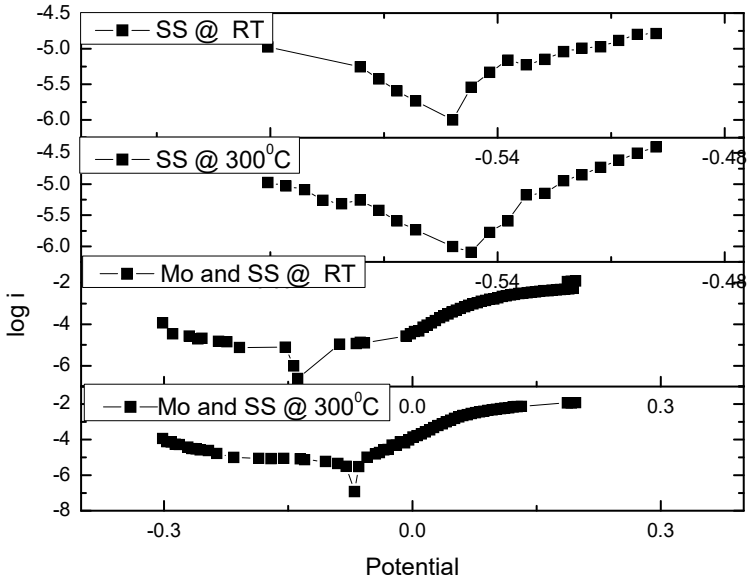

Fig. 9. Analysis of Corrosion Resistance Behaviour

The SS thin film sample deposited at room temperature shows low charge transfer resistance (R_{CT} – 1) at higher frequency, compared to the thin film coated at higher temperature. This may be because of the higher concentration of Fe grains rather than other phases.

In the case of SS-Mo thin films deposited at room temperature, the charge transfer resistance in the higher frequency is almost equal or fairly larger than that of the SS deposited at room temperature. The increment in the corrosion resistance of the SS-Mo composite could be attributed to the presence of Mo along with Fe phase. The molybdenum remains electrochemically inactive and present in between the Fe phase and thus reduces the contagious oxidation of Fe phase. Hence the realization of SS-Mo composite has resulted in better corrosion resistance. The higher frequency charge transfer resistance of the SS-Mo film deposited at 300°C is still larger than all the films and it could be solely attributed to the successful formation of SS-Mo thin film composite (SS-Mo TFC).

From the observed results, the deviation in the corrosion potential may be corroborated to the more inert nature of the thin films. Hence, it may be concluded that the deposition of SS and SS-Mo composite films at high temperature results in better corrosion proof coatings as shown in Table 10.

Hence, the corrosion resistance of the films can be arranged in the following order: **SS-Mo films deposited @ 300°C >> SS films deposited @ 300°C > SS-Mo films deposited @ RT > SS films deposited @ RT.**

5. Conclusion

In this work, SS and SS-Mo composite thin films have been prepared on a copper substrate (for corrosion testing) and glass substrate (for structural, morphological and chemical composition) using an indigenously prepared DC sputtering target. The sputtering target is created by tiling Mo metal sheets with an area of 9.8 cm^2, and they are chopped from a 3 mm thick Mo sheet (Sigma Aldrich; Purity 99.99%), on the SS target. The sputtering yields of SS and Mo are 429 A^0/min and 421 A^0/min, respectively to realize thin films with 1:1 SS to Mo ratio. The composition of the stainless steel target has been analyzed through Energy Dispersive X ray absorption spectrometer.

The sputtering has been carried out under different conditions: (a) deposition of SS target at room temperature (b) deposition of SS target at 300°C (c) deposition of Mo embedded SS target at room temperature and (d) deposition of Mo embedded SS target at 300°C. From the XRD results it is clearly evident that the deposition of SS substrate at room temperature is devoid of Chromium and Nickel phase, and it may also be concluded that deposition at 300°C results in composition closer to SS target whereas Molybdenum remains in an amorphous state between SS layers. In order to further confirm the presence of Molybdenum along with SS phase, EDX analysis has been performed and from the EDX results, it may be concluded that the sputtering deposition from Mo embedded SS target at 300°C is a facile way to develop Thin film nano composites of Fe-Cr-Ni-C and Mo phases.

Further, the Annual corrosion rate is calculated from the TAFEL polarization and Electrochemical Impedance Spectroscopy (EIS) measurements. From the observed results, deviation in the corrosion potential may be corroborated by the more inert nature of the SS-Mo thin films. Hence, it may be concluded that the deposition of SS and SS-Mo composite films at high temperature results in better corrosion proof coatings which are validated by the proposed SEM analysis methods where Molybdenum increases corrosion resistance at high temperature. Eventually, these surface modifications can influence electrochemical behaviour and, therefore, corrosion susceptibility is demonstrated by laboratory experiments. In the present work, a novel texture – morphology based feature descriptor has been developed to characterize corrosion resistance behavior. For this, feature selection and feature weighting methods have been carried out to empirically derive the corrosion resistance behavior directly from the imagery. Further a machine learning algorithm, SVM has been employed to analyze the SEM image of the prepared composite at normal and elevated temperatures. This Non-destructive way of testing is also inferring that the SS-Mo coatings deposited at 300°C provide superior corrosion resistance properties which matches with laboratory results.

REFERENCES

[1] S. Hanish Anand, T. Subash Murugan, S. Shanmuga Pandian, Fabrication and Mechanical Testing Of Mmc Formed By Reinforcement of Alumina & Graphite in Aluminium LM 24, International Journal of Emerging Technology in Computer Science & Electronics (IJETCSE) **21**, 3 (2016).

[2] G.R. Raghav, N. Selvakumar, K. Jeyasubramanian, M.R. Thansekhar, Corrosion analysis of copper – TiO2 nanocomposite coatings on steel using sputtering, International Journal of Innovative Research in Science, Engineering and Technology **3**, 3 (2014),

[3] Liu Rong, Jianhua Yao, Qunli Zhang, Matthew, X. Yao, Rachel Collier, Effects of molybdenum content on the wear/erosion and corrosion performance of low-carbon Stellite alloys, Materials & Design **78**, 95-106 (2015).

[4] M.C. Thirumoolam, B. Sivaramakrishnan, M. Devarajan, Sputtering deposition of aluminium molybdenum alloy thin film anodes for thin film microbatteries, Electronic Materials Letters **11**, 3, 416-423 (2015).

[5] I.B. Singh, M. Singh, S. Das, A comparative corrosion behavior of Mg, AZ31 and AZ91 alloys in 3.5% NaCl solution, Journal of Magnesium and Alloys **3**, 2, 142-148 (2015).

[6] S. Zhang, S. Wang, C.L. Wu, C.H. Zhang, M. Guan, J.Z. Tan, Cavitation erosion and erosion-corrosion resistance of austenitic stainless steel by plasma transferred arc welding, Engineering Failure Analysis **76**, 115-124 (2017).

[7] E. Jafari, Corrosion behaviors of two types of commercial stainless steel after plastic deformation, Journal of Materials Science & Technology **26**, 9, 833-838 (2010).

[8] T.M. Chandran, S. Balaji, Sputtering Deposition of Sn–Mo-Based Composite Anode for Thin-Film Li-Ion Batteries, Journal of Electronic Materials **45**, 6, 3220-3226 (2016).

[9] M.S. Priyan, P. Hariharan, Wear and Corrosion Resistance of Fe Based Coatings by HVOF Sprayed on Gray Cast-Iron for Automotive Application, Tribology in Industry **36**, 4 (2014).

[10] I. Sulima, P. Putyra, P. Hyjek, T. Tokarski, Effect of SPS parameters on densification and properties of steel matrix composites, Advanced Powder Technology **26**, 4, 1152-1161 (2015).

[11] D. Dwivedi, K. Lepková, T. Becker, Carbon steel corrosion: a review of key surface properties and characterization methods, RSC Advances **7**, 8, 4580-4610 (2017).

[12] N.A. Otsu, Threshold selection method from gray-level histograms, IEEE Transactions on Systems, Man, and Cybernetics **9**, 1, 62-6 (1979).

[13] S. Sridhar, 'Digital Image Processing', Oxford University Press (2011).

[14] Chaplot Sandeep, L.M. Patnaik, N.R. Jagannathan, Classification of magnetic resonance brain images using wavelets as input to support vector machine and neural network, Biomedical Signal Processing and Control **1**, 1, 86-92 (2006).

[15] M.C. Pravin, S. Karthikeyan, B. Sathyabama, D.S. Vinothini, Texture and morphology based conductivity analysis of fuel cell-bipolar plate using scanning electron microscopic images, Indian Journal of Engineering & Materials Sciences **24**, 261-269 (2017).

[16] M. Şenel, M. Gürbüz, Investigation on Mechanical Properties and Microstructures of Aluminum Hybrid Composites Reinforced with Al 2 O 3/GNPs Binary Particles, Archives of Metallurgy and Materials **66** (2021).

[17] S. Manigandan, T.R Praveenkumar, A.M. Al-Mohaimeed, K. Brindhadevi, A. Pugazhendhi, Characterization of polyurethane coating on high performance concrete reinforced with chemically treated Ananas erectifolius fiber, Progress in Organic Coatings **150**, 105977 (2021).

[18] G. Pitchamuthu, M. Sekar, A. Anderson, D, Jayakumar, Evaluation of iron-epoxy metal nanocomposite in glass fibre and Kevlar, International Journal of Ambient Energy **39** (2), 122-126 (2018).

[19] R.C. De Amorim, B. Mirkin, Minkowski metric, feature weighting and anomalous cluster initializing in K-Means clustering, Pattern Recognition **45** (3), 1061-1075 (2012).

[20] K. Uma, B. Sathya Bama, D. Sabarinathan, Identification and retrieval of medicinal plants from Southern India using Efficient-B4Net, Journal of Intelligent & Fuzzy Systems, (Preprint), 1-16. (2022).